Low-Complexity Iterative MMSE-PIC Detection for MIMO-GFDM

Maximilian Matthé, Dan Zhang, Gerhard Fettweis
Vodafone Chair Mobile Communication Systems,
Technische Universität Dresden, Germany
{maximilian.matthe,dan.zhang,fettweis}@ifn.et.tu-dresden.de

***Abstract*—Driven by 5G requirements, research on alternatives to the popular cyclic-prefix orthogonal frequency division multiplexing (CP-OFDM) waveform recently arose. In particular, non-orthogonal circularly filtered waveforms such as generalized frequency division multiplexing (GFDM) were proposed due to flexibility and robustness. Applying multiple-input multiple-output (MIMO) techniques for future wireless networks is unquestionable and thereby compulsory for any alternative waveform. Despite advancements in accurate MIMO detection algorithms for GFDM, compared to CP-OFDM their complexity still exhibited a higher order of magnitude, impeding an energy-efficient implementation. In this paper, we propose a low-complexity formulation for iterative minimum mean squared error with parallel interference cancellation (MMSE-PIC) detection for non-orthogonal waveforms with localized inter-carrier interference (ICI), where we focus on the application to MIMO-GFDM. The proposal achieves complexity similar to CP-OFDM and we analyze its performance under realistic channel conditions with imperfect channel state information, where we obtain up to 2dB gain of GFDM compared to OFDM. We confirm our findings by analyzing the measured extrinsic information transfer (EXIT) charts and show that the proposal achieves the performance of optimal maximum likelihood (ML) detection. The results point out the MMSE-PIC algorithm as a viable technique for iterative MIMO receiver implementations for non-orthogonal waveforms.**

***Index Terms*—Spatial Multiplexing, interference, low-complexity, waveform, iterative processing**

I. Introduction

Requirements of future wireless communication systems will go beyond an increased data rate. Low latency transmissions, asynchronous multiple access, heterogeneous network architectures, and massively increased number of connected devices pose strong challenges on the underlying physical layer (PHY) of the system [1], [2]. As was shown numerous times, cyclic-prefix orthogonal frequency division multiplexing (CP-OFDM), despite its energy-efficient implementation and simple equalization, cannot cope with the challenging requirements for future networks [3], [4]. Hence, alternative waveforms have been in the focus of academic research in the last years [3], including non-orthogonal waveforms such as generalized frequency division multiplexing (GFDM) [5] or cyclic-block filtered multitone (CB-FMT) [6].

An important aspect in the research on alternative waveforms concerns multiple-input multiple-output (MIMO) capability, as MIMO techniques are mandatory for nowaday's and future wireless communications. Compared to the straightforward implementation for CP-OFDM, non-orthogonality of filtered multicarrier waveforms can significantly complicate the MIMO operation. Despite, a theoretic analysis on capacity bounds of non-orthogonal waveforms and OFDM in frequency-selective MIMO channels [7] revealed a higher capacity for non-orthogonal systems.

However, as the standardization for fifth generation (5G) cellular proceeds, filtered and windowed variants of CP-OFDM were agreed on by industry consortiums [8], [9], [10]. They will be at the core of the 5G celluar PHY for enhanced mobile broadband (eMBB) use cases. The main focus of current research towards standardization is the reduction of out-of-band (OOB) emissions. Reduced OOB emission can improve spectral efficiency by reducing the number of required guard carriers [11] and provide more robustness for asynchronous transmissions by reducing inter-user interference [10]. As this goal can be already reached by simple signal processing such as filtering and windowing, the choice of waveforms derived from CP-OFDM by filtering or windowing appears natural for early releases of 5G cellular standards, since frame structure, synchronization and channel estimation algorithms can mostly remain compared to 4G solutions. However, a common drawback of these waveforms is the inflexible constraint of transmitting each data point over a single frequency bin. This can lead to suboptimal performance in severely frequency selective channels [7]. In this context, advanced non-orthogonal waveforms circumvent this constraint by spreading each data point over multiple frequency bins. However, at the same time inter-symbol interference (ISI), inter-carrier interference (ICI) and, in case of MIMO systems, inter-antenna interference (IAI) can occur, such that the design of an optimal receiver can lead to impractical complexity. Hence, to make non-orthogonal waveforms viable for practical use, it is of major importance to design low-complexity receivers that achieve close-to-optimal performance. The work in this paper is motivated by this premise and we provide a step forward for implementing these receivers with complexity that is affordable on today's hardware. Despite being generically applicable for non-orthogonal multicarrier waveforms, we focus our presentation on GFDM.

In the literature, numerous algorithms for detecting spatially multiplexed GFDM have been proposed. But, for non-iterative schemes, GFDM generally performed worse than OFDM [12], [13], [14], [15]. Compared to the orthogonal CP-OFDM, the difficulty for MIMO detection for GFDM is the occurence of 3-dimensional interference, namely ISI, ICI and IAI. In order to achieve optimal detection performance, this interference

needs to be jointly equalized. This was not achieved in [12], [13], [14], [15] and hence the potential of GFDM in MIMO applications was not fully exploited. Iterative receivers [16], [17] for MIMO-GFDM, based on a soft-input soft-output (SISO) GFDM demapping unit and a SISO forward error correction (FEC) channel decoder, outperformed optimally performing OFDM schemes in terms of frame error rate (FER) under artificial channels with severe power delay profiles. In this paper, we focus on the well-accepted iterative minimum mean square error (MMSE) parallel interference cancellation (PIC) algorithm for MIMO detection. There have been various implementation proposals in the literature [18], [19], [20], offering competent performance and complexity against non-linear MIMO demapping schemes such as sphere decoding [21], [22]. Closely related, the authors in [23] proposed a decision feedback equalizer (DFE) system for single-carrier MIMO systems, which, as we show below, is equivalent to MMSE-PIC. In [24], we proposed an efficient implementation of non-iterative linear minimum mean square error (LMMSE) receiver that permits the performance gain of GFDM over OFDM with comparable complexity. However, the LMMSE receiver is still far from the optimum in theory. Therefore, in this work, we aim at extending it to MMSE-PIC for achieving close-to-optimal performance.

The contribution of this paper is two-fold: First, we extend the proposal from [24] for iterative MMSE-PIC equalization and eventually achieve comparable complexity to an equivalent OFDM implementation. The proposal bases on a sparse factorization of the equivalent channel matrix, which allows to jointly treat interference in three steps that can be approximated with low-complexity Fourier transforms. We show that the performance loss in terms of coded FER due to this approximation is negligible. Compared to an existing implementation of the MMSE-PIC algorithm in [25], we significantly reduce the complexity order from cubic to quasi-linear in the number of interfering symbols.

Second, we contribute a thorough analysis of the performance of iterative MMSE-PIC demapping for GFDM under realistic channel conditions. As the performance of a system does depend on the joint behaviour of waveform and channel code, we additionally analyze the performance of different FEC methods, namely low-density parity check (LDPC) channel codes with sum-product algorithm (SPA) SISO decoding and convolutional codes (CCs) with Bahl-Cocke-Jelinek-Raviv (BCJR) SISO decoding.To this end, we present simulation results of the proposed algorithm employing both LDPC codes and CCs in realistic channel conditions with imperfect channel state information (CSI). In particular, we compare the performance of iterative and non-iterative receivers for MIMO-GFDM and MIMO-OFDM in extended vehicular-A (EVA) and extended typical urban (ETU) channels with mobility. By means of analysis of extrinsic information transfer (EXIT) charts, we show that the LDPC code is not suitable for iterative detection. In contrast, identifying the system as a serially concatenated code with the MIMO constellation constraint being the outer code and the FEC constituting the inner code, high performance with iterative decoding with SISO inner (i.e. BCJR) and outer (i.e. MMSE-PIC) decoders can be expected [26]. We confirm these findings with extensive numerical simulations.

The remainder of this paper is organized as follows. Sec. II introduces the system model and shortly summarizes MMSE-PIC SISO demapping. In Sec. III, we employ a sparse factorization of the GFDM system matrix, yielding a 3-step estimation process for SISO MMSE-PIC detection. In Sec. IV, we analyze the complexity of each estimation step and propose approximations to reduce complexity to an equal level as OFDM. Sec. V presents simulation results of the proposed algorithms and, finally, the conclusions are drawn in Sec. VI.

Notation: Matrices and vectors are written in boldface and with arrow as $\mathbf{X}, \vec{x}$. $\mathrm{diag}(\mathbf{X})$ denotes the diagonal of the matrix $\mathbf{X}$ and $\mathrm{diag}(\vec{x})$ returns a diagonal matrix with diagonal $\vec{x}$. $\mathrm{circ}(\vec{v})$ returns a circulant Toeplitz matrix with $\vec{v}$ as its first column. $\mathrm{vec}(\mathbf{X})$ performs vectorization of the matrix $\mathbf{X}$, i.e. stacking the columns of $\mathbf{X}$ on top of each other. $\mathbb{C}$ denotes the set of complex numbers. $\mathcal{CN}(\vec{\mu}, \Sigma)$ describes a complex normal distribution with mean $\vec{\mu}$ and covariance Σ.

II. System Model

A. MIMO-GFDM Transmitter And Wireless Channel

Consider a $N_R \times N_T$ spatial multiplexing MIMO GFDM system. The MIMO channel consists of $N_T N_R$ i.i.d. multipath fading processes associated to each transmit receive antenna pair. As we assume the transmitter has no prior channel knowledge, equal power allocation for the transmit antennas is applied. GFDM is a block-based multicarrier scheme. Subsequent blocks are separated by a CP which mitigates inter-block interference (IBI). In each GFDM block, with length of $N = M \cdot K$ samples, $N_{on} = M \cdot K_{on}$ complex-valued constellation symbols are transmitted, divided into M subsymbols on K_{on} subcarriers. K is the overall number of available subcarriers in a GFDM block. A detailed description of GFDM itself is beyond the scope of this paper, but we refer the readers to e.g. [5] and references therein.

Following [27], the transmit signal $\mathbf{X}$ for all antennas before CP insertion can be written as

$$\mathbf{X} = \mathbf{A} \underbrace{[\vec{d}_1, \vec{d}_2, \ldots, \vec{d}_{N_T}]}_{\mathbf{d} \in \mathbb{C}^{N_{on} \times N_T}} \tag{1}$$

where $\mathbf{A}$ is the $N \times N_{on}$ GFDM time domain modulation matrix and $\vec{d}_t$ are column vectors with the constellation symbols to be modulated on the tth antenna.

We denote the block discrete Fourier transform (DFT) matrix $\mathbf{T} = \mathbf{F}_M \otimes \mathbf{I}_{K_{on}}$ with $\mathbf{F}_M$ being the unitary M-point DFT matrix. We transform the transmit signal into frequency domain by

$$\mathbf{F}_N \mathbf{X} = \mathbf{F}_N \mathbf{A} \mathbf{T}^{\mathrm{H}} \mathbf{T} \mathbf{d} \tag{2}$$

$$= \mathbf{A}_f \mathbf{D}, \tag{3}$$

with $\mathbf{D} = \mathbf{T}\mathbf{d}$ being the M-DFT of the M subsymbols on each subcarrier. Moreover, as shown in [24], $\mathbf{A}_f = \mathbf{F}_N \mathbf{A} \mathbf{T}^{\mathrm{H}}$ is equivalent to a block diagonal matrix consisting of M bidiagonal blocks of size $K \times K_{on}$ after appropriate row- and column-wise permutations. Accordingly, the solution of a linear system involving $\mathbf{A}_f$ can be calculated from M

bidiagonal equation systems of size $K \times K_{on}$. This property will be a key ingredient for the complexity reduction in Sec. IV.

Assume a block-fading channel and the CP is longer than the channel impulse response (CIR). With perfect synchronization, the channel between each pair of transmit and receive antennas becomes circulant in time and hence diagonal in the frequency. After passing through the MIMO multipath fading channel and AWGN, the received signal in the frequency domain equals

$$\vec{y} = \underbrace{\begin{pmatrix} \mathbf{H}_{11} & \dots & \mathbf{H}_{1N_T} \\ \vdots & \ddots & \vdots \\ \mathbf{H}_{N_R1} & \dots & \mathbf{H}_{N_RN_T} \end{pmatrix} (\mathbf{I}_{N_T} \otimes \mathbf{F}_N \mathbf{A}) \operatorname{vec}(\mathbf{d})}_{\tilde{\mathbf{H}}} + \vec{n} = \tilde{\mathbf{H}}\vec{d} + \vec{n}, \tag{4}$$

$$= \underbrace{\begin{pmatrix} \mathbf{H}_{11} & \dots & \mathbf{H}_{1N_T} \\ \vdots & \ddots & \vdots \\ \mathbf{H}_{N_R1} & \dots & \mathbf{H}_{N_RN_T} \end{pmatrix} (\mathbf{I}_{N_T} \otimes \mathbf{A}_f) \operatorname{vec}(\mathbf{D})}_{\mathbf{H}} + \vec{n} = \mathbf{H}\vec{D} + \vec{n}, \tag{5}$$

where $\mathbf{H}_{rt}$ is the diagonal channel matrix between the tth transmit and rth receive antenna. We assume uncorrelated transmit symbols of unit energy, i.e. $E[\vec{d}\vec{d}^{\mathrm{H}}] = \mathbf{I}$, normalized channels, i.e. $E[\mathrm{tr}(\mathbf{H}_{rt}\mathbf{H}_{rt}^{\mathrm{H}})] = N$, and $\vec{n}$ is additive white Gaussian noise (AWGN) according to $\vec{n} \sim \mathcal{CN}(0, \sigma_n^2\mathbf{I})$. Note that in mobile channels, the condition of block-fading does only approximately hold, as the channel changes during the transmission depending on the channel Doppler spread. However, due to simplicity reasons but at the cost of performance, the receiver assumes a constant channel during transmission. We will investigate the resulting performance degradation in the simulation results in Section V.

B. Component-wise Conditionally Unbiased (CWCU) LMMSE Estimation

As commonly known, the conventional LMMSE estimator is conditionally biased towards the a-priori knowledge of the estimand [28]. Here, we introduce our notation for the LMMSE estimation and summarize equations for an unbiased relative, namely the CWCU LMMSE estimator. Θ_x denotes the LMMSE estimator that calculates an estimate of $\vec{x}$ from the measurement $\vec{y}$ from the linear model $\vec{y} = \mathbf{H}\vec{x} + \vec{n}$ with a-apriori knowledge on $\vec{x}$ and $\vec{n}$ as

$$\vec{x} \sim \mathcal{CN}(\vec{\mu}_x^a, \Sigma_x^a) \qquad \vec{n} \sim \mathcal{CN}(\vec{0}, \Sigma_n^a). \tag{6}$$

Let (η_x^p, Λ_x^p) denote the LMMSE estimate and error variance of this estimate for $\vec{x}$ and denote the LMMSE estimation operation by

$$(\vec{\eta}_x^p, \Lambda_x^p) = \Theta_x[\vec{y} = \mathbf{H}\vec{x} + \vec{n}, \mathcal{CN}(\vec{\mu}_x^a, \Sigma_x^a), \mathcal{CN}(\vec{0}, \Sigma_n^a)]. \tag{7}$$

Here, the first, second and third arguments to Θ_x are the linear model with known $\vec{y}$ and $\mathbf{H}$, the a-priori information on $\vec{x}$ and the a-priori information on the noise $\vec{n}$, respectively. Then, Θ_x generates the LMMSE estimate and error covariance matrix by the common LMMSE operation:

$$\vec{\eta}_x^p = \vec{\mu}_x^a + \Sigma_x^a\mathbf{H}^{\mathrm{H}}(\mathbf{H}\Sigma_x^a\mathbf{H}^{\mathrm{H}} + \Sigma_n^a)^{-1}(\vec{y} - \mathbf{H}\vec{\mu}_x^a) \tag{8}$$

$$\Lambda_x^p = \Sigma_x^a - \Sigma_x^a\mathbf{H}^{\mathrm{H}}(\mathbf{H}\Sigma_x^a\mathbf{H}^{\mathrm{H}} + \Sigma_n^a)^{-1}\mathbf{H}^{\mathrm{H}}\Sigma_x^a. \tag{9}$$

This estimation is conditionally biased since $E[\vec{\eta}_x^p|\vec{x}] \neq \vec{x}$. This is due to the fact that the effective channel matrix after filtering, i.e. $\Sigma_x^a\mathbf{H}^{\mathrm{H}}(\mathbf{H}\Sigma_x^a\mathbf{H}^{\mathrm{H}} + \Sigma_n^a)^{-1}\mathbf{H}$, does not have a unit diagonal. In predating works [25], [18], this bias was taken care of in the log-likelihood ratio (LLR) calculation by including the effective channel gain into the expressions. However, we can directly overcome this bias by calculating a CWCU LMMSE estimator [29] Φ_x of $\vec{x}$ given by

$$(\vec{\mu}_x^p, \Sigma_x^p) = \Phi_x[\vec{y} = \mathbf{H}\vec{x} + \vec{n}, \mathcal{CN}(\vec{\mu}_x^a, \Sigma_x^a), \mathcal{CN}(\vec{0}, \Sigma_n^a)], \tag{10}$$

where the outcome of (10) is defined by

$$\vec{\mu}_x^p = \vec{\mu}_x^a + \frac{\mathbf{H}^{\mathrm{H}}(\mathbf{H}\Sigma_x^a\mathbf{H}^{\mathrm{H}} + \Sigma_n^a)^{-1}(\vec{y} - \mathbf{H}\vec{\mu}_x^a)}{\mathrm{diag}[\mathbf{H}^{\mathrm{H}}(\mathbf{H}\Sigma_x^a\mathbf{H}^{\mathrm{H}} + \Sigma_n^a)^{-1}\mathbf{H}]} \tag{11}$$

$$\text{and } \mathrm{diag}(\Sigma_x^p) = \frac{\vec{1}}{\mathrm{diag}[\mathbf{H}^{\mathrm{H}}(\mathbf{H}\Sigma_x^a\mathbf{H}^{\mathrm{H}} + \Sigma_n^a)^{-1}\mathbf{H}]} - \mathrm{diag}[\Sigma_x^a]. \tag{12}$$

Here, the division of vector by vector is carried out element-wise. For the CWCU estimator, we only provide the diagonal elements of the a-posteri covariance matrix Σ_x^p of $\vec{x}$ in a simple form since for our purposes, considering the diagonal of the covariance is sufficient. However, in general this does not mean that the CWCU estimation provides uncorrelated estimates. More details about CWCU estimation, including the exact expression for Σ_x^p can be found in [30].

C. Iterative Detection Based On MMSE-PIC Demapping

In this section, we summarize the common framework of iterative MMSE-PIC SISO demapping, which has previously been studied in e.g. [18], [31], [25] and references therein. The central unit in the SISO demapping process is an LMMSE estimator, that utilizes a-priori information coming from the output of a channel decoder to provide refined information based on the (known) channel input/output relation. In particular, the overall demapping operation is split into 3 steps:

1) *Obtaining soft QAM constellation symbols from the channel decoder LLR.* Let $x_{s,b} \in \{0, 1\}$ be the bth bit of the sth constellation symbol and let its a-priori information be encoded in the LLR value $L_{s,b}^A$ with $Pr[x_{s,b} = 1] = \frac{1}{1+\exp(L_{s,b}^A)}$. Then, mean and variance of the a-priori constellation symbols are given by [18]

$$(\vec{\mu}_d^a)_s = \sum_{d\in\mathcal{S}} Pr[d_s = d]d = \sum_{d\in\mathcal{S}} \prod_b Pr[x_{s,b} = \mathcal{X}_b^{-1}(d)]d$$
$$(\Sigma_d^a)_{ss} = \sum_{d\in\mathcal{S}} Pr[d_s = d]\|d - (\vec{\mu}_d^a)_s\|^2, \tag{13}$$

where $Pr[d_s = d]$ is calculated from the product of the corresponding $Pr[x_{s,b} = \mathcal{X}_b^{-1}(d)]$ and the QAM-to-bit mapping $\mathcal{X}_b^{-1}(d)$ yields the bth bit of the complex

constellation symbol d. In the initial iteration no channel decoder feedback is available, i.e. $\vec{\mu}_d^a = 0$ and $\Sigma_d^a = \mathbf{I}$.

2) *Refining the constellation symbols* by performing CWCU LMMSE estimation with the received signal

$$(\vec{\mu}_d^p, \Sigma_d^p) = \Phi_d[\vec{y} = \tilde{\mathbf{H}}\vec{d} + \vec{n}, \mathcal{CN}(\vec{\mu}_d^a, \Sigma_d^a), \mathcal{CN}(\vec{0}, \sigma_n^2\mathbf{I})]. \tag{14}$$

Note that in previous papers, the bias originating from the LMMSE estimation was removed in the following demapping operation. In the present paper we directly remove the bias by employing the CWCU estimation. Both techniques are numerically equilavent, but the latter is more suitable for the formulation used in this paper.

3) *Obtaining LLR from the LMMSE estimation result.* Here, an approximation is made by assuming that the noise on each constellation symbol is independent[25]. Furthermore, optimally the a-priori knowledge on each bit is included in the demapping process, however in [18] it was shown that omitting the a-priori knowledge has only marginal impact on the overall performance for SISO MMSE-PIC demapping. Accordingly, the demapping operation for each constellation symbol is given by [18]

$$L_{s,b}^E = \frac{1}{(\Sigma_d^p)_{ss}} \left(\min_{d \in \mathcal{S}_b^{(0)}} |(\vec{\mu}_d^p)_s - d|^2 - \min_{d \in \mathcal{S}_b^{(1)}} |(\vec{\mu}_d^p)_s - d|^2 \right) \tag{15}$$

where $\mathcal{S}_b^{(0)}$ and $\mathcal{S}_b^{(1)}$ denote the set of constellation symbols where the bth bit is 0 or 1, respectively. Afterwards, the LLRs are sent to the channel decoder to estimate the transmitted code word.

D. Relation to Iterative Decision Feedback Equalization

In this section, we establish a relation between this work and the DFE algorithm in [23], that was tailored for single-carrier MIMO systems. Even though [23] does not start from the MMSE-PIC perspective, the following derivation shows the equivalence of [23] and MMSE-PIC. Instead, [23] performs iterative detection in combination with feedforward and feedback filtering the received signal and decoder output, respectively, as exemplified by (cf. eq. (6) in [23])

$$\vec{\mu}_d^p = \mathbf{W}\vec{y} - \mathbf{V}\vec{\mu}_d^a. \tag{16}$$

There, $\mathbf{W}$ and $\mathbf{V}$ are the feedforward and feedback filter matrices for the current iteration. These are designed to minimize $E[\|\vec{d} - \vec{\mu}_d^p\|^2]$, i.e. they follow the MMSE criterion. Particular attention is paid on avoiding self-subtraction by the feedback filter by imposing the constraint $\text{diag}(\mathbf{V}) = \vec{0}$. To show the equivalence to MMSE-PIC, we start from (14) to get

$$\vec{\mu}_d^p = \vec{\mu}_d^a + \mathbf{E}^{-1}\tilde{\mathbf{H}}^{\mathrm{H}}(\tilde{\mathbf{H}}\Sigma_d^a\tilde{\mathbf{H}}^{\mathrm{H}} + \sigma_n^2\mathbf{I})^{-1}(\vec{y} - \tilde{\mathbf{H}}\vec{\mu}_d^a), \tag{17}$$

with $\mathbf{E}$ being a diagonal matrix compensating the bias of LMMSE estimation with

$$\text{diag}(\mathbf{E}) = \text{diag}[\tilde{\mathbf{H}}^{\mathrm{H}}(\tilde{\mathbf{H}}\Sigma_d^a\tilde{\mathbf{H}}^{\mathrm{H}} + \sigma_n^2\mathbf{I})^{-1}\tilde{\mathbf{H}}]. \tag{18}$$

Defining the overall filter matrix $\tilde{\mathbf{W}}$ as

$$\tilde{\mathbf{W}} = \mathbf{E}^{-1}\tilde{\mathbf{H}}^{\mathrm{H}}(\tilde{\mathbf{H}}\Sigma_d^a\tilde{\mathbf{H}}^{\mathrm{H}} + \sigma_n^2\mathbf{I})^{-1}, \tag{19}$$

we reformulate (17) to

$$\vec{\mu}_d^p = \vec{\mu}_d^a + \tilde{\mathbf{W}}(\vec{y} - \tilde{\mathbf{H}}\vec{\mu}_d^a) = \tilde{\mathbf{W}}\vec{y} - (\tilde{\mathbf{W}}\tilde{\mathbf{H}} - \mathbf{I})\vec{\mu}_d^a, \tag{20}$$

which shows the relation to the DFE technique from [23]. First, we can identify the feedforward filter of the DFE as $\mathbf{W} = \tilde{\mathbf{W}}$. Moreover, the feedback filter is given by $\mathbf{V} = \tilde{\mathbf{W}}\tilde{\mathbf{H}} - \mathbf{I}$, which also fulfills the constraint $\text{diag}(\tilde{\mathbf{W}}\tilde{\mathbf{H}} - \mathbf{I}) = \vec{0}$. The authors in [23] propose a low-complexity frequency domain formulation of the DFE technique which is suitable for the system model suffering from IAI and ISI. In this paper we propose to reduce MMSE-PIC demapping complexity for MIMO multicarrier systems which are subject to additional ICI due to non-orthogonal subcarriers. Therefore, in the following sections we first propose a formulation to split the MMSE-PIC demapping problem into three steps and subsequently propose approximate methods to solve them in a pipelined and parallelized fashion.

III. LMMSE Estimation With Factorized System Matrix

The direct solution of (14) for MIMO-GFDM has been approached by us in [25] where we could solve the MMSE-PIC problem with complexity $\mathcal{O}(K_{on}M^3N_T^2N_R)$ due to the banded structure of the system. In this section, we propose a novel 3-step factorization of the LMMSE estimation problem by introducing an intermediate variable $\vec{D}$. $\vec{D}$ is unitarily equivalent to the actual estimand $\vec{d}$, but its intermediate estimation allows us to reduce complexity to $\mathcal{O}(K_{on}M\log(M)N_T^2N_R)$ in Sec. IV. This factorization, which is based on the structure and locality of the interference, is presented in the following. Starting from the linear model

$$\vec{y} = \tilde{\mathbf{H}}\vec{d} + \vec{n} \tag{21}$$

we need to obtain the CWCU estimate of $\vec{d}$, given by

$$(\vec{\mu}_d^p, \Sigma_d^p) = \Phi_d[\vec{y} = \tilde{\mathbf{H}}\vec{d} + \vec{n}, \mathcal{CN}(\vec{\mu}_d^a, \Sigma_d^a), \mathcal{CN}(\vec{0}, \sigma_n^2\mathbf{I})]. \tag{22}$$

However, instead of directly estimating $(\vec{\mu}_d^p, \Sigma_d^p)$ in (22), we can resort to the data in the frequency domain $\vec{D} = \mathbf{U}\vec{d}$ with $\mathbf{U} = \mathbf{I}_{N_T} \otimes \mathbf{T}$ (cf. (5)). Accordingly, the a-priori mean $\vec{\mu}_D^a$ and covariance Σ_D^a of $\vec{D}$ are given by

$$\vec{\mu}_D^a = \mathbf{U}\vec{\mu}_d^a, \qquad \Sigma_D^a = \mathbf{U}\Sigma_d^a\mathbf{U}^{\mathrm{H}}. \tag{23}$$

We can now get the CWCU estimate of $\vec{D}$ from

$$(\vec{\mu}_D^p, \Sigma_D^p) = \Phi_D[\vec{y} = \mathbf{H}\vec{D} + \vec{n}, \mathcal{CN}(\vec{\mu}_D^a, \Sigma_D^a), \mathcal{CN}(\vec{0}, \sigma^2\mathbf{I})] \tag{24}$$

Note, that under the constraint that Σ_D^a is a diagonal matrix, the equation system in (24) decays into M band-diagonal systems each of size N_TK_{on} where the (one-sided) bandwidth is N_T, as was shown in [32], [24]. Moreover, we can show that with a diagonal Σ_D^a we have (cf App. A)

$$(\eta_d^p, \Lambda_d^p) = \Theta_d[\vec{\mu}_D^p = \mathbf{U}\vec{d} + \vec{n}, \mathcal{CN}(\vec{\mu}_d^a, \Sigma_d^a), \mathcal{CN}(\vec{0}, \Sigma_D^p)], \tag{25}$$

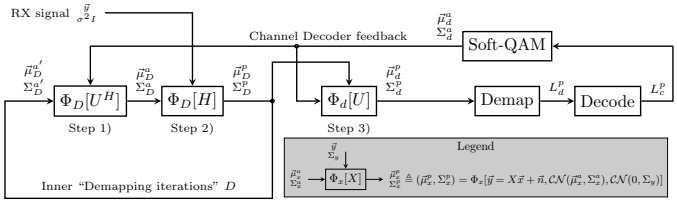

Fig. 1. Block diagram of the 3-step MMSE estimation process in combination with channel decoder.

i.e. the (biased) a-posteriori LMMSE estimate of $\vec{d}$ can be calculated from the CWCU a-posteriori LMMSE estimate of $\vec{D}$ with the linear model $\vec{\mu}_D^p = \mathbf{U}\vec{d} + \vec{\eta}$ where $\vec{\eta}$ contains the uncertainty of the a-posteriori $\vec{D}$. By analogy, the final a-posteriori CWCU estimate for $\vec{d}$ is calculated by

$$(\vec{\mu}_d^p, \Sigma_d^p) = \Phi_d[\vec{\mu}_D^p = \mathbf{U}\vec{d} + \vec{\eta}, \mathcal{CN}(\vec{\mu}_d^a, \Sigma_d^a), \mathcal{CN}(\vec{0}, \Sigma_D^p)]. \tag{26}$$

The above derivation has assumed that the covariance matrix Σ_D^a is diagonal, which, according to (23), requires the variances of Σ_d^a to be equal on one subcarrier. Practically, this constraint is only fulfilled, when $\Sigma_d^a = \mathbf{I}$, i.e. in the initial iteration, when no decoder feedback is available[1]. The constraint is violated with feedback information from the channel decoder, as the channel code intentionally combines bits from different carriers to gain frequency diversity. In this case, by analogy to the estimation of $(\vec{\mu}_d^p, \Sigma_d^p)$ from $(\vec{\mu}_D^p, \Sigma_D^p)$ in (26), we resort to CWCU LMMSE estimation of $(\vec{\mu}_D^a, \Sigma_D^a)$ from the a-priori knowledge $(\vec{\mu}_d^a, \Sigma_d^a)$, given by

$$(\vec{\mu}_D^a, \Sigma_D^a) = \Phi_D[\vec{\mu}_d^a = \mathbf{U}^{\mathrm{H}}\vec{D} + \vec{\eta}, \mathcal{CN}(\vec{\mu}_D^{a'}, \Sigma_D^{a'}), \mathcal{CN}(\vec{0}, \Sigma_d^a)]. \tag{27}$$

Here, $(\vec{\mu}_D^{a'}, \Sigma_D^{a'})$ is some a-priori knowledge on the distribution of $\vec{D}$. In the simplest case we have $(\vec{\mu}_D^{a'}, \Sigma_D^{a'}) = (\vec{0}, \mathbf{I})$, however below we introduce the concept of inner demapping operations to reliably resolve the approximation error by supplying more accurate $(\vec{\mu}_D^{a'}, \Sigma_D^{a'})$.

Accordingly, we can split the overall MMSE-PIC detection process into 3 steps:

1) Calculate $(\vec{\mu}_D^a, \Sigma_D^a)$ as the CWCU LMMSE estimate of $\vec{D}$ from the model $\vec{\mu}_d^a = \mathbf{U}^{\mathrm{H}}\vec{D} + \vec{\eta}$, $\vec{\eta} \sim \mathcal{CN}(\vec{0}, \Sigma_d^a)$ and $(\vec{\mu}_D^{a'}, \Sigma_D^{a'})$.
2) Calculate $(\vec{\mu}_D^p, \Sigma_D^p)$ as the CWCU LMMSE estimate of $\vec{D}$ from the received signal $\vec{y} = \mathbf{H}\vec{D} + \vec{n}$ and $(\vec{\mu}_D^a, \Sigma_D^a)$.
3) Calculate $(\vec{\mu}_d^p, \Sigma_d^p)$ as the CWCU LMMSE estimate of $\vec{d}$ from the model $\vec{\mu}_D^p = \mathbf{U}\vec{d} + \vec{\eta}$, $\vec{\eta} \sim \mathcal{CN}(\vec{0}, \Sigma_D^p)$ and $(\vec{\mu}_d^a, \Sigma_d^a)$.

We want to emphasize that, despite this treatment focuses on the application to GFDM, the proposed 3-step estimation technique to first estimate DFT-transformed data symbols can readily be employed for other non-orthogonal waveforms with localized ICI which obey the linear model (21). For the case of no a-priori knowledge, this has already been demonstrated in [24]. The present extension of transforming a-priori knowledge from the time to the frequency domain and vice versa can be straight-forwardly applied to other waveforms.

Note, that in case of $\mathbf{U}^{\mathrm{H}}\Sigma_d^a\mathbf{U}$ being diagonal, the CWCU LMMSE estimate of $(\vec{\mu}_D^a, \Sigma_D^a)$ in (27) and the direct transform from time to frequency in (23) are equivalent. However, in case of Σ_D^a not being diagonal, the LMMSE estimation process tends to produce less correlated estimates, compared to the operation in (23) and hence provides more decoupled values to step 2). Nethertheless, the final LMMSE estimate of $\vec{d}$ will not be exact due to ignored correlation between frequency-domain data $\vec{D}$. In order to mitigate this problem, it is possible to perform D inner demapping iterations between steps 1) and 2), where the output $(\vec{\mu}_D^p, \Sigma_D^p)$ of step 2) can serve as a-priori knowledge $(\vec{\mu}_D^{a'}, \Sigma_D^{a'})$ for step 1). This way, the estimation performance can be improved, at the cost of increased complexity. However, depending on the number of these iterations, this operation can also lead to suboptimal convergence.

Fig. 1 illustrates the contained loops, LMMSE estimation blocks and overall receiver structure for the proposed detection algorithm. Using the information from the channel decoder, $(\vec{\mu}_d^a, \Sigma_d^a)$ is generated by soft-modulating the respective a-posteriori LLRs as in (13). Then, this information is used to acquire $(\vec{\mu}_D^a, \Sigma_D^a)$ in step 1) which is in turn used to gain improved knowledge $(\vec{\mu}_D^p, \Sigma_D^p)$ in step 2). Finally, this information is transformed to $(\vec{\mu}_d^p, \Sigma_d^p)$ in step 3) and forwarded to the constellation demapper as in (15) and the channel decoder, closing the iteration loop.

IV. Approximate Solution And Complexity Assessment

This section proposes an approximation to the SISO MMSE-PIC demapping operation for GFDM to reduce complexity and improve parallelizability. Considering Fig. 1, the 3 steps for the LMMSE estimation need to be carried out sequentially, hence in order to reduce latency, each step should be fast and parallelizable.

A. Steps 1) and 3): Transforming frequency to time-domain data and vice versa

Initially, in (27) in step 1) a CWCU LMMSE estimation of the frequency domain data based on the time-domain data is to be calculated by

$$\begin{aligned} \vec{\mu}_D^a &= \vec{\mu}_D^{a'} + \frac{(\Sigma_D^{a'} + \mathbf{U}\Sigma_d^a\mathbf{U}^{\mathrm{H}})^{-1}(\mathbf{U}\vec{\mu}_d^a - \vec{\mu}_D^{a'})}{\mathrm{diag}((\Sigma_D^{a'} + \mathbf{U}\Sigma_d^a\mathbf{U}^{\mathrm{H}})^{-1})} \\ \Sigma_D^a &= \frac{1}{\mathrm{diag}((\Sigma_D^{a'} + \mathbf{U}\Sigma_d^a\mathbf{U}^{\mathrm{H}})^{-1})} - \Sigma_D^{a'}. \end{aligned} \tag{28}$$

Note that since $\mathbf{U} = \mathbf{I}_{N_T} \otimes \mathbf{F}_M \otimes \mathbf{I}_{K_{on}}$, (28) can be decoupled into $N_T K_{on}$ smaller systems of size $M \times M$ with coefficient matrices $\{\mathbf{X}_{kt}\}_{k=0,\ldots,K_{on}-1;t=0,\ldots,N_T-1}$ given by

$$\mathbf{X}_{kt} = \Sigma_{D,kt}^{a'} + \mathbf{F}_M\Sigma_{d,kt}^a\mathbf{F}_M^{\mathrm{H}} = \Sigma_{D,kt}^{a'} + \mathrm{circ}\left(\tfrac{1}{\sqrt{M}}\mathbf{F}_M\mathrm{diag}(\Sigma_{d,kt}^a)\right). \tag{29}$$

In (29), the index $(\cdot)_{kt}$ denotes to select the M elements that correspond to the kth subcarrier from the tth transmit antenna.

[1]To be precise, Σ_D^a can also be diagonal, if the decoder is in overall very confident and the covariance becomes close to zero. However, in this case, the detection problem is already solved by having found the correct code word.

Calculating the numerator in (28) requires to solve $\mathbf{X}_{kt}^{-1}\vec{b}$ for the right-hand side $\vec{b} = \mathbf{U}\vec{\mu}_d^a - \vec{\mu}_D^{a'}$, whereas the denominator requires knowledge of $\text{diag}(\mathbf{X}_{kt}^{-1})$. Even though $\mathbf{X}_{kt}$ is a highly structured matrix by being the sum of a positive definite diagonal and circulant matrix $\mathbf{C}+\mathbf{D}$, no specific solvers for these kinds of systems exist in the literature. Most closely, in [33] an algorithm for systems of the form $(\mathbf{C}+j\mathbf{D})$ is presented, where $\mathbf{C}$ has eigenvalues with positive real part and $\mathbf{D}$ is real-valued. Hence, in order to not be restricted by the $\mathcal{O}(M^3)$ complexity of brute-force matrix inversion, we resort to approximate methods.

Let us first consider $\text{diag}(\mathbf{X}_{kt}^{-1})$. As shown in the following, we can approximate $\vec{x}_{k,t} = \text{diag}(\mathbf{X}_{kt}^{-1})$ by $\vec{x}'_{kt}$ given by

$$\text{diag}(\mathbf{X}_{kt}^{-1}) = \vec{x}_{kt} \approx \vec{x}'_{kt} = \text{diag}((\Sigma_{D,kt}^{a'} + \tfrac{1}{M}\text{tr}(\Sigma_{d,kt}^{a})\mathbf{I})^{-1}) \tag{30}$$

from the observation that the diagonal of $\mathbf{X}_{kt}$ is larger than its off-diagonal elements.

We assume the elements $\sigma_{d,i}^2$ of $\Sigma_{d,kt}^a$ are i.i.d. random variables that are distributed according to some distribution[2]. Since $\sigma_{d,i}^2 \in (0,1]$ they have non-zero mean and we can model

$$\sigma_{d,i}^2 = \bar{\sigma}_d^2 + r_i \tag{31}$$

$$r_i \sim \mathcal{D}(\sigma_r^2), \tag{32}$$

where $\bar{\sigma}_d^2$ is the mean of the a-priori variance information of $\vec{d}$ and r_i follows some zero-mean distribution with variance σ_r^2. Note that due to the boundedness of $\sigma_{d,i}^2 \in (0,1]$, σ_r^2 is limited by $\sigma_r^2 \leq r_{\max}^2$ with $r_{\max} = \min(\bar{\sigma}_d^2, 1-\bar{\sigma}_d^2)$. The corner case $\sigma_r^2 = r_{\max}^2$ corresponds to a degenerate distribution of maximum variance with density $p(r) = \frac{1}{2}(\delta(r-r_{\max})+\delta(r+r_{\max}))$. We can now calculate the expected value of the first column $\vec{c}_1$ of the circulant matrix $\mathbf{F}_M\Sigma_{d,kt}^a\mathbf{F}_M^{\text{H}}$ by

$$\bar{\vec{c}}_1 = E[\vec{c}_1] = \tfrac{1}{\sqrt{M}}\mathbf{F}_M E[\text{diag}(\Sigma_{d,kt}^a)] = \bar{\sigma}_d^2\vec{e}_1, \tag{33}$$

which holds because of the identity $\frac{1}{\sqrt{M}}\text{circ}(\mathbf{F}_M\vec{v}) = \mathbf{F}_M\text{diag}(\vec{v})\mathbf{F}_M^{\text{H}}$ for any $M-$dimensional vector $\vec{v}$ and $E[\text{diag}(\Sigma_{d,kt}^a)] = \bar{\sigma}_d\vec{1}$. There, $\vec{e}_1$ is the first column of an $M\times M$ identity matrix. Furthermore, the variance on each element of $\vec{c}_1$ is given by

$$E[(\vec{c}_1-\bar{\vec{c}}_1)(\vec{c}_1-\bar{\vec{c}}_1)^{\text{H}}] = \sigma_r^2\mathbf{I}. \tag{34}$$

Hence, on average $\vec{c}_1$ equals $\bar{\sigma}_d^2\vec{e}_1$ and each element varies with standard deviation $\sigma_r < \bar{\sigma}_d^2$, which is less than the mean of the first element of $\vec{c}_1$. Eventually, we can conclude that the diagonal of $\mathbf{X}_{kt}$ is larger than its off-diagonal elements and the expression in (30) approximately holds, where we have estimated the true mean $\bar{\sigma}_d^2$ from the elements of $\Sigma_{d,kt}^a$ by $\bar{\sigma}_d^2 \approx \frac{\text{tr}(\Sigma_{d,kt}^a)}{M}$.

Figure 2 numerically evaluates the normalized approximation error ρ_{kt} of (30) given by

$$\rho_{kt} = E\left[\frac{\|\vec{x}_{kt}-\vec{x}'_{kt}\|^2}{\|\vec{x}_{kt}\|^2}\right]. \tag{35}$$

[2]Considering that the a-priori knowledge for the demapper is generated from the channel decoder including a possible interleaver, this assumption is valid.

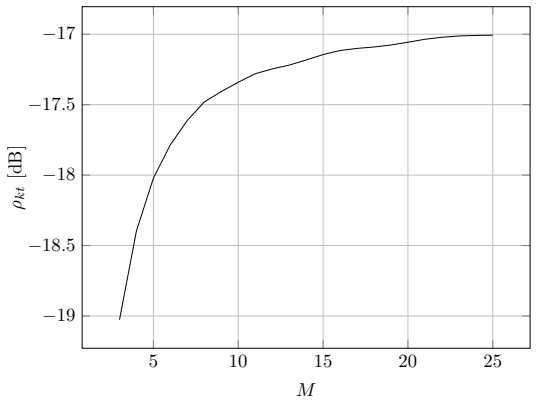

Fig. 2. Numerical evaluation of MSE ρ_{kt} of approximation of $\vec{x}_{kt}$ with $\vec{x}'_{kt}$, given by (35). In the simulation, the diagonal of both $\Sigma_{d,kt}^a$ and $\Sigma_{D,kt}^{a'}$ contain independent uniformly distributed entries in the range $(0,1]$.

Notably, the approximation error increases with the system size M. Qualitatively, we can explain this observation by the uncertainty incorporated by the approximation. An accurate calculation of $\vec{x}_{kt}$ considers $2M$ parameters (M variables on the diagonals of both $\Sigma_{d,kt}^a$ and $\Sigma_{D,kt}^{a'}$), whereas the approximation $\vec{x}'_{kt}$ only uses $M+1$ variables (M diagonal entries of $\Sigma_{D,kt}^{a'}$ and $\text{tr}(\Sigma_{d,kt}^a)$) to estimate $\vec{x}'_{kt}$. However, within the analyzed range of M the normalized squared error remains below -17dB[3] and hence the approximated diagonal $\vec{x}'_{kt}$ is 2% close to the correct diagonal $\vec{x}_{kt}$.

For efficiently calculating the solution to $\mathbf{X}_{kt}^{-1}\vec{b} = (\mathbf{C}+\mathbf{D})^{-1}\vec{b}$, we note that multiplying with a diagonal matrix is trivial and for a circulant matrix it can be done with quasilinear complexity via the DFT. Accordingly, we can employ the iterative conjugate gradient (CGD) method [34], which converges quickly to the exact solution. However, by being integrated in an iterative overall detection process, it might even not be necessary to find the exact solution to (28) in each outer iteration, but an approximate solution suffices.

Tab. I outlines the process for solving the system $(\Sigma_{D,kt}^{a'} + \mathbf{F}_M\Sigma_{d,kt}^a\mathbf{F}_M^{\text{H}})^{-1}(\mathbf{F}\vec{\mu}_{d,kt}^a - \vec{\mu}_{D,kt}^{a'})$ of step 1) with the CGD method and summarizes the required number of operations for each step. As the CGD method requires an initial starting point for the iterations, we use the approximate inverse in (30) to calculate an initial solution. The same algorithm can also be used for step 3) of the LMMSE estimation process, by replacing the corresponding variables. Note that in the last iteration, only the first two steps of the loop are necessary, since the remaining steps yield values for the following iteration. We finally note that all $N_T K_{on}$ small $M\times M$ systems are independent and can be solved in parallel, making it suitable for a parallelized implementation.

[3]Evaluations for larger M show that ρ_{kt} is bounded by -16.5dB, not shown in the figure.

TABLE I
ALGORITHM DESCRIPTION OF THE CONJUGATE GRADIENT METHOD FOR LMMSE STEPS 1) AND 3). DFT DENOTES THE OPERATION COUNT FOR AN M-POINT DFT, I.E. $M \log M$ COMPLEX OPERATIONS, WHICH IS QUASILINEAR IN M.

Calculation	Add.	Mult.	Div.	DFT
$\vec{b} = \mathbf{F}_M \vec{\mu}^a_{d,kt} - \vec{\mu}^{a'}_{D,kt}$	M			
$\vec{x}_0 = (\Sigma^{a'}_{D,kt} + \frac{\mathrm{tr}(\Sigma^a_{d,kt})}{M}\mathbf{I})^{-1}\vec{b}$	$2M-1$	0	$M+1$	
$\vec{r}_0 = \vec{b} - (\Sigma^{a'}_{D,kt} + \mathbf{F}_M \Sigma^a_{d,kt} \mathbf{F}^{\mathrm{H}}_M)\vec{x}_0$	$2M$	$2M$	0	
$\vec{p}_0 = \vec{r}_0, k = 0$				
Repeat				
$\alpha_k = \frac{\vec{r}^{\mathrm{H}}_k \vec{r}_k}{\vec{p}^{\mathrm{H}}_k (\Sigma^{a'}_{D,kt} + \mathbf{F}_M \Sigma^a_{d,kt} \mathbf{F}^{\mathrm{H}}_M)\vec{p}_k}$	$4M-2$	$4M$	1	
$\vec{x}_{k+1} = \vec{x}_k + \alpha_k \vec{p}_k$	M	M	0	
$\vec{r}_{k+1} = \vec{r}_k - \alpha_k (\Sigma^{a'}_{D,kt} + \mathbf{F}_M \Sigma^a_{d,kt} \mathbf{F}^{\mathrm{H}}_M)\vec{p}_k$	M	M	0	
$\beta_k = \frac{\vec{r}^{\mathrm{H}}_{k+1} \vec{r}_{k+1}}{\vec{r}^{\mathrm{H}}_k \vec{r}_k}$	$M-1$	M	1	
$\vec{p}_{k+1} = \vec{r}_{k+1} + \beta_k \vec{p}_k$	M	M	0	
$k = k+1$				
Overall count $K_{Max} = 1$	$10M-3$	$7M$	$M+2$	3
Overall count $K_{Max} = 2$	$18M-6$	$15M$	$M+4$	5
Overall count $K_{Max} = 5$	$42M-15$	$39M$	$M+10$	13

TABLE II
GFDM AND OFDM CONFIGURATION USED IN THE SIMULATION.

Parameter	Symbol	GFDM	OF
# Available Subcarriers	K	128	15
# Allocated Subcarriers	K_{on}	3 or 24	$12 \cdot \{$
# Subsymbols	M	12	
# Allocated Subsymbols	M_{on}	12	
# Tx, Rx antennas	T, R	4	
Prototype filter	$g[n]$	RC	R
Filter rolloff	α	0 or 1	
CP length	-	4.7μs (EVA channel); 16.7μ	
Time-Window	-	RC window, 16 samp	
Modulation and coding	-	{(16-QAM, $r = 1/2$),(64-Q	
Channel Model		3GPP EVA, ETU; $f_d = \{0, 30, 100\}$Hz,	
CSI		Perfect CSI or Imperfect CSI: Channel	
LDPC Code		WiMax LDPC with SPA log-MA	
Convolutional Code	$\{133, 171\}_8$	recursive systematic CC (RSCC) w	
# GFDM/OFDM blocks per frame	F	LDPC: 8; Con	

B. Step 2): LMMSE estimation for frequency domain data

According to the results in [25], the LMMSE estimation process for step 2) can be written as

$$\vec{\mu}^p_D = \vec{\mu}^a_D + \frac{(\mathbf{H}^{\mathrm{H}}\mathbf{H}\Sigma^a_D + \sigma^2\mathbf{I})^{-1}(\mathbf{H}^{\mathrm{H}}\vec{y} - \mathbf{H}^{\mathrm{H}}\mathbf{H}\vec{\mu}^a_D)}{\mathrm{diag}((\mathbf{H}\mathbf{H}^{\mathrm{H}}\Sigma^a_D + \sigma^2\mathbf{I})^{-1}\mathbf{H}^{\mathrm{H}}\mathbf{H})}$$
$$\Sigma^p_D = \frac{1}{\mathrm{diag}((\mathbf{H}^{\mathrm{H}}\mathbf{H}\Sigma^a_D + \sigma^2_n\mathbf{I})^{-1}\mathbf{H}^{\mathrm{H}}\mathbf{H})} - \Sigma^a_D. \quad (36)$$

As shown in [24], the equation system in (36) is equivalent to M systems of size $N_T K_{on}$ each, where each equation system is governed by a band-diagonal matrix with (single-sided) bandwidth $B = N_T$. However, this only exactly holds, if Σ^a_D is a diagonal matrix, which is the case when no decoder feedback was incorporated into the demapping operation. In any other case, we approximate the solution by ignoring the off-diagonal elements of Σ^a_D and still consider the systems separately. Then, following [25] for a band-diagonal system, we perform the estimation with complexity $\mathcal{O}(K_{on}N_R N_T^2)$ for each of the M systems. Since the systems are decoupled, all systems can be solved in parallel, creating no extra penalty on the overall latency.

C. Overall Complexity

Let $\mathcal{O}(F_N)$ denote the arithmetic complexity of an N-point FFT, which we approximate by $\mathcal{O}(F_N) \approx \mathcal{O}(N \log N)$. Considering the straight-forward implementation of the SISO MMSE-PIC demapping operation for OFDM with symbol length MK where MK_{on} subcarriers are allocated, the order of complexity in terms of arithmetic operations can be estimated by

$$C_{OFDM} = N_R \mathcal{O}(F_{KM}) + IMK_{on}\mathcal{O}(N_R N_T^2) \quad (37)$$

where I denotes the number of MMSE-PIC iterations. There, the first term corresponds to the transformation of the received time-domain signal into the frequency domain. The second term describes the complexity of the MK_{on} LMMSE inversions of the $N_R \times N_T$ channel matrix of each subcarrier, which need to be carried out in each iteration. Now, considering the arithmetic complexity for GFDM with K_{on} allocated subcarriers, we end up with

$$C_{GFDM} = N_R \mathcal{O}(F_{KM}) + I(N_T K_{on}\mathcal{O}(F_M) + M\mathcal{O}(K_{on}N_R N_T^2) + N$$
(38)

Again, the first term corresponds to the transformation of the received time-domain signal to the frequency domain. The second, third and fourth term correspond to steps 1), 2) and 3) of the MMSE-PIC demapping for each iteration, respectively. In total, we find

$$C_{OFDM} = N_R \mathcal{O}(F_{MK}) + IMK_{on}\mathcal{O}(N_R N_T^2) \quad (39)$$
$$C_{GFDM} = N_R \mathcal{O}(F_{MK}) + IM\mathcal{O}(K_{on}N_R N_T^2) + 2IN_T K_{on}\mathcal{O}(F_M), \quad (40)$$

showing that the proposed algorithm for GFDM has only a quasi-linear overhead in number of symbols and streams compared to OFDM and in complete both systems exhibit the similar order of complexity in terms of big-O notation. Compared to the solution provided in [25], where the complete system using $\tilde{\mathbf{H}}$ was solved at once with complexity

$$C_{GDFM,[25]} = N_R \mathcal{O}(F_{MK}) + I\mathcal{O}(K_{on}M^3 N_R N_T^2), \quad (41)$$

the current proposal offers linear complexity in the number of active subcarriers K_{on} and quasi-linear complexity $O(M \log M)$ in the number of subsymbols M which is a significant gain compared to the cubic complexity in M obtained in [25]. Furthermore potential for high-level pipelining and parallelism for a practical implementation is readily available by splitting the estimation process into 3 sequential steps, with each step consisting of independent systems.

V. SIMULATION RESULTS

In this section we present performance simulation results of the proposed algorithms using a 4x4 MIMO system under realistic Long-Term Evolution (LTE) EVA and ETU channel models as defined by 3GPP with mobility and maximum delay spread of 2.5μs and 5μs, respectively. Tab. II shows the simulation parameters that have been adopted in the present

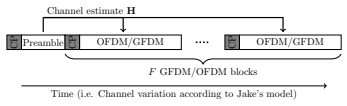

Fig. 3. Frame structure.

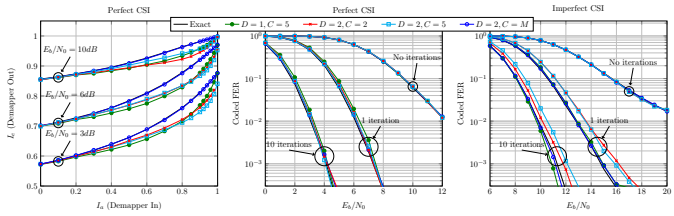

Fig. 4. Performance of the approximate solution with DFT-spread detection and internal demapper iterations. ETU power delay profile with $F_D = 30Hz$; 16-QAM $r = 0.5, \alpha = 1, K_{on} = 3$.

simulation. The GFDM parameters are derived from an OFDM LTE system with 15MHz bandwidth with sampling frequency of 23.04MHz. We have made GFDM and OFDM blocks of equal length and 12 subsymbols are contained in one GFDM block. Hence, one GFDM subcarrier has the width of one LTE physical resource block (PRB). Additionally, to be in line with commonly applied OOB reduction methods, we have added a raised cosine time-window of length of 16 samples to each OFDM and GFDM block, to emulate a windowed-GFDM [35] or windowed-OFDM [11] scheme. The frame structure of the adopted scheme is shown in Fig. 3, where F GFDM or OFDM blocks are preceded by a single preamble, that is used for channel estimation. The channel was implemented using Jake's model with a given Doppler spread, i.e. the channel was time-variant. However, the CSI for the receiver was obtained only from the preamble and assumed to be constant during the full frame. We have performed simulations with perfect and imperfect CSI where we emulate the channel estimation by supplying erroneous CSI to the demapping unit. Assuming an LMMSE channel estimation unit has knowledge of the power delay profile (PDP), the channel estimate is given by adding random noise of variance depending on the signal-to-noise ratio (SNR) to the correct impulse response, i.e. $\vec{h} = \hat{\vec{h}} + \vec{n}_h$ where $\hat{\vec{h}}$ is the obtained CSI and $\vec{h}$ is the average impulse response during the preamble. Further, $\vec{n}_h \sim \mathcal{CN}(\vec{0}, \sigma_h^2)$ is the channel estimation error. The SNR is defined as $\frac{1}{\sigma_n^2} = \mu r \frac{E_b}{N_0}$ and for imperfect CSI we have $\sigma_h^2 = \sigma_n^2/2$. For perfect CSI, we set $\sigma_h^2 = 0$.

Fig. 4 compares the performance of the approximate solution of the LMMSE estimation process by doing the estimation in the symbol's frequency domain as described in Sec. IV against the exact detection. The figure shows both the measured information transfer curves as well as the obtained FER performance with perfect and imperfect CSI. The information transfer curves depict the mutual information between the coded bits and the output of the demapper. Therefore, they describe the amount of the code bit information that is accessible by the demapper through the channel observation and the a-priori information. In other words, the information transfer curves describe the information gained by the demapper from the received signal, when provided a given amount of a-priori information. Using information transfer curves, the behaviour under iterative detection methods can be inferred. For more information on information transfer charts, we refer the reader to [36], [37]. In Fig. 4 all information transfer curves start in the same point, and the FER performance of all schemes is equal with no iterations, confirming that the 3-step estimation process is exact when no a-priori knowledge is available in the system.

When decoder feedback is available, with perfect CSI the performance of the approximate methods is only slightly worse than the exact solution. A very different result occurs for the more realistic case of imperfect CSI as a performance difference of almost 1.5dB at a FER of 10^{-3} can be observed. In particular, performing no extra demapping iterations ($D = 1$) and using the approximate CGD method with $C = 5$ CGD iterations even outperforms the exact MMSE-PIC SISO demapper in terms of FER. We can explain this behaviour by the fact that the exact MMSE-PIC demapper does not consider imperfect CSI, but only considers the noise term in the calculation of a-posteriori LLR. As such, the exact SISO demapper tends to be over-confident with imperfect CSI and the iterative receiver might get stuck in a local minimum and does not necessarily reach the optimum solution. In contrast, the approximate method with $D = 1, C = 5$ introduces approximation errors into the system, which occur as extra noise at the demapper. This extra noise can reduce the over-confidence and hence aids in reaching a more optimal solution. The parametrization $D = 2, C = M$ yields a performance close to the exact solution, showing that this configuration approximates the exact MMSE-PIC demapping accurately. On the other hand, the parametrizations $D = 2, C = \{2 \text{ or } 5\}$ perform $\approx$ 1dB worse than the exact SISO MMSE-PIC demapping. To conclude, we find that performing internal demapping operations ($D > 1$) in combination with an exact solution of (28) yields a performance that is close to the direct solution of (22). In contrast, for imperfect CSI the parametrization $D = 1, C = 5$ even outperforms the direct solution of (22) in terms of FER at lower complexity. With perfect CSI, there is only a marginal difference between all investigated parametrizations. Hence, in the following evaluations, we employ the parametrization $D = 1, C = 5$ if not otherwise stated.

Fig. 5 shows the information transfer chart of the SISO MMSE-PIC demapper for GFDM and OFDM in a block-fading ETU channel. Confirming the results in [25], the GFDM and OFDM curves intersect and the intersection moves left with increasing SNR, exhibiting potential that iterative GFDM schemes can outperform iterative OFDM schemes. However, the effect is not as pronounced as in [25], due to significantly less frequency diversity in the more realistic ETU channel. Interestingly, for $E_b/N_0 = 15$dB, the starting point of the GFDM curve is above the OFDM curve, indicating that already a non-iterative GFDM LMMSE receiver can outperform OFDM. Additionally, Fig. 5 presents the information transfer chart for the BCJR decoder of the employed $\{133, 171\}_8$ RSCC and the sum-product algorithm (SPA) decoder of the

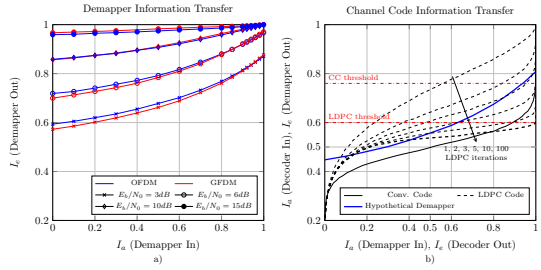

Fig. 5. Information transfer chart of the SISO demapper in block-fading ETU channel a) with perfect CSI, $\alpha = 1$ and $K_{on} = 3$ and SISO channel decoders b) with code rate $r = \frac{1}{2}$. GFDM employs the direct solution of (22).

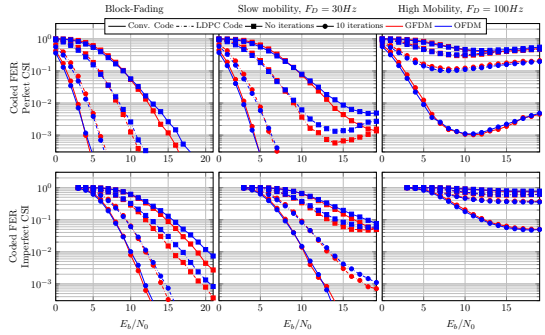

Fig. 6. Performance of convolutional and LDPC channel codes with and without MMSE-PIC iterations. Here, the channel exhibits an EVA power delay profile, assuming both perfect and imperfect CSI. $r = \frac{1}{2}, \alpha = 1, K_{on} = 3$.

WiMax LDPC code. For the SPA, the characteristic for different SPA iteration counts are shown. As shown, the SPA performance improves with more iterations, and accordingly we chose to use 100 iterations for the subsequent FER performance measurements. Comparing the shape of the channel decoder and demapper curves, it becomes apparent why an LDPC channel code does not perform well with the iterative detection scheme, but well with non-iterative detection.

The curve of the more powerful LDPC code in general proceeds steeper and more horizontally than that of the CC, as is shown in Fig. 5b. Hence, as soon as the input information I_a (y-Axis in Fig. 5b) exceeds a certain threshold, which is roughly $I_a \geq 0.6$ for the used LDPC code, the SPA can recover the transmitted codeword. The CC requires approximately $I_a \geq 0.76$ to successfully decode a received codeword. Hence, in a non-iterative scheme the LDPC code will significantly outperform the CC as it essentially needs a lower starting point of the demapper curve and hence lower SNR for a successful decoding.

However, the picture changes in an iterative detection setting, where the channel decoder and demapper exchange information. In this case, in principle successful decoding is possible when the tunnel between demapper and decoder curves is open [36]. Fig. 5b shows a hypothetic demapper curve showing an open tunnel between the CC and demapper curve. The tunnel is closed when considering the LDPC code. Accordingly, we expect a superior behaviour of the CC compared to the LDPC code when operating in iterative detection.

Note, that above statements only have qualitative value, as the EXIT chart analysis requires infinitely long codewords with perfect interleaving, which is certainly not fulfilled in the present setup. For more information on using the EXIT chart with finite code words we refer the reader to e.g. [38]. Our findings are confirmed in existing literature, where it has been shown in e.g. [21] that the CC decoder exhibits a better energy consumption-performance tradeoff compared to more powerful channel codes when employed in iterative receiver structures. Moreover, the authors in [39] designed irregular CCs that significantly outperformed more powerful Turbo and LDPC codes in iterative detection settings in combination with MIMO demappers. In fact, the combination of the MIMO constellation constraint and the CC can be considered as a serially concatenated code [26], which can, in contrast to a single CC, result in compelling FER performance [40]. Hence, for the upcoming FER performance simulations, we expect the CC to outperform the LDPC code in an iterative receiver context. On the other hand, with no iterations, the LDPC code is expected to outperform the CC due to its steeper EXIT curve, once the initial input I_a threshold is exceeded.

Fig. 6 shows the performance of the LMMSE and MMSE-PIC receivers with CC and LDPC channel codes for block-fading and time-varying EVA channels with perfect and imperfect CSI. As qualitatively derived from Fig. 5, for a non-iterative LMMSE detector, the LDPC code outperforms the CC by approximately 4dB for a FER of 10^{-2} in the block-fading case for perfect CSI. On the contrary, with the MMSE-PIC detector, the CC performs better after convergence, outperforming the LDPC code by 1.5dB for a FER of 10^{-2}. In overall, for block-fading channels a gain of 5dB is achieved for MMSE-PIC detection with CCs compared to non-iterative detection employing LDPC codes. The gain increases when the Doppler spread of the channel increases. Similar observations can be done for the case of imperfect CSI, where all curves are shifted approximately 7dB to the right. We have obtained similar relations between LDPC and CCs before and after convergence for different code rates, power delay profiles and doppler spreads and perfect and imperfect CSI (not shown). Accordingly, in the subsequent figures we focus on the LDPC code for the non-iterative receiver, whereas we employ CCs for the iterative receiver.

When comparing the performance between GFDM and OFDM in Fig. 6, we find that for the non-iterative case, GFDM shows a steeper slope in the FER curve, eventually crossing the OFDM curve, which can again be explained with the findings from Fig. 5. Accordingly, GFDM outperforms OFDM by roughly 0.8dB at FER=10^{-3} in the block-fading case for perfect CSI. For imperfect CSI we can observe a greater robustness of GFDM against imperfect CSI and GFDM outperforms OFDM by 1dB at FER=10^{-3}. With $f_d = 30$Hz, the effect is emphasized and also the error floor for GFDM due to the time-variant channel is reduced. When $f_d = 100$Hz, the channel varies too quickly, the CSI soon becomes outdated and reliable detection with the employed frame structure and channel estimation is not feasible. Even, for SNR>10dB, the FER increases with SNR. We can explain this behaviour with

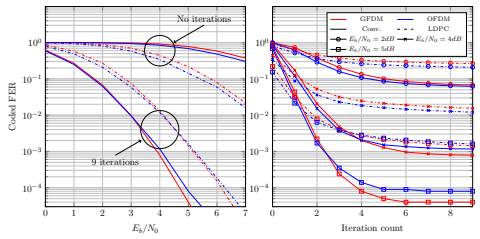

Fig. 7. Convergence behaviour of GFDM and OFDM. Code rate $r = 0.5, \alpha = 1, K_{on} = 3$, ETU power delay profile, block-fading channel with perfect CSI.

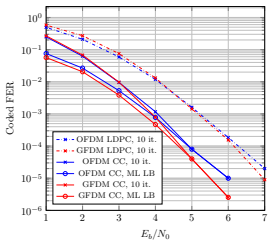

Fig. 9. ML lower bound for the GFDM and OFDM. ETU power delay profile with static block-fading, $r = 0.5, \alpha = 1, K_{on} = 3$.

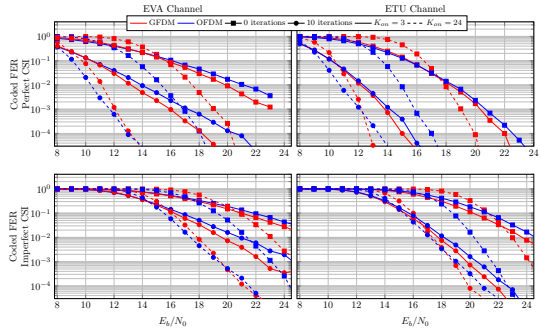

Fig. 8. FER performance for 64QAM modulation, code rate $r = 3/4$ and $\alpha = 1$ for EVA and ETU block fading channels. The rate $3/4$ CC was obtained by puncturing the original half-rate code with the puncturing pattern $[1, 1, 0, 1, 1, 0]$.

the demapper being too confident due to the low noise variance since it does not consider the time-variance of the channel. This leads to poor information sent to the channel decoder which eventually degrades FER performance.

Fig. 7 compares the convergence of the iterative receivers for GFDM and OFDM in an ETU block fading channel, using CC and LDPC codes. As shown, with no iterations, the LDPC code outperforms the CC, however its gain during iterations is below that of the CC, eventually performing inferior than a CC. In addition, it is shown that for few iterations (<3), OFDM performs superior than GFDM. Though, for more iterations, GFDM converges to a lower FER, eventually outperforming OFDM after 4 iterations and converging at 8 iterations. These findings emphasize the necessity of an iterative receiver for GFDM in order to beneficially consider the additional ICI and ISI.

Fig. 8 compares the FER performance for a higher modulation and coding scheme (MCS), namely 64-QAM and $r = 3/4$, in block-fading EVA and ETU channels with perfect and imperfect CSI. Additionally, we have simulated a system with more allocated subcarriers, i.e. $K_{on} = 24$. To this end, we have extended the CC codeword to span all available resources. For the LDPC code, due to its limited configuration options, we have concatenated several LDPC code words of length 2016 bits and interleaved them over all subcarriers and subsymbols such that each codeword experiences the same frequency diversity.

First, comparing the ETU and EVA channels, we observe a steeper slope in the FER curves for the ETU channel. This can be straight-forwardly explained by the larger frequency diversity of the ETU channel. Additionally, comparing the curves for $K_{on} = 3$ with $K_{on} = 24$ we observe a steeper slope for the $K_{on} = 24$ curve. Again, this is explained by a bigger frequency diversity when a codeword can span more subcarriers. A fundamental difference between GFDM and OFDM can be observed when considering the non-iterative LMMSE receiver for $K_{on} = 24$: Despite GFDM was outperforming OFDM for $K_{on} = 3$, for $K_{on} = 24$ GFDM performs more than 2dB worse than OFDM and the slope of both curves is equal. We can explain this by the increased amount of self-interference in GFDM when $K_{on} = 24$. In this case, the LMMSE equalizer cannot reliably resolve the interference and the performance degrades. In contrast, comparing the performance of the iterative schemes, we observe that for $K_{on} = 24$ GFDM shows a steeper slope in the FER curve compared to OFDM. This indicates that the iterative GFDM receiver can harvest more frequency diversity from the multipath channel due to the wider subcarriers. Eventually, in the ETU channel GFDM outperforms OFDM for FER=10^{-4} by 1dB for both perfect and imperfect CSI. In the EVA channel, OFDM performs superior than GFDM until FER=10^{-4}. Again, these findings emphasize the statement [13] that only an iterative receiver scheme can exploit the foreseen performance gain for GFDM in frequency selective channels [7], by beneficially considering the self-interference. In fact, these observations point out an important tradeoff of non-orthogonal waveforms which are polluted by self-interference: If the receiver is capable of accurately resolving the interference e.g. using iterative detection, more self-interference yields superior performance, since the inner part of the serial code concatenation becomes stronger. However, in case the interference cannot be resolved as with the non-iterative LMMSE receiver, self-interference can severely degrade the FER performance since it eventually appears as extra noise after equalization.

Considering the optimally achievable maximum likelihood (ML) performance, Fig. 9 presents the obtained FER performance of the converged OFDM and GFDM demodulators along with an ML performance lower bound that was obtained with a genie-aided technique as in [17]: Upon convergence of the detection, the distance d_R of the detected codeword to the received signal is compared to the distance d_T of the transmitted codeword to the received signal. If $d_R < d_T$, an optimal ML detector would also yield an error. If $d_R > d_T$, it is assumed that an optimal ML detector would have found the correct solution. This process overestimates the performance of the ML detector and hence yields a lower bound

on ML decoding performance. The tightness of the bound becomes better, when the detection algorithm approaches the ML decoding performance. As is shown in Fig. 9, the MMSE-PIC detector approaches the ML bound for higher SNR when using the convolutional code. The obtained results show that the proposed iterative detection algorithms achieve the optimal performance for the given signal structure when using a convolutional code. Further, the ML bound for the GFDM system is roughly 0.5dB left to the OFDM ML bound, showing the benefits of frequency diversity and ICI for higher SNR. With an LDPC code, the ML bound could not be calculated with the proposed technique, since the obtained FER performance was too far away from the optimal ML performance. In particular, the lower bound estimate was FER>0, since for each erroneously detected frame we experienced $d_R > d_T$ in the LDPC coded case. Here, we again see the superiority of the CC compared to the LDPC code, as the CC reaches the optimally achievable performance in the considered iterative receiver due to its interaction with the SISO MMSE-PIC demapper.

VI. Conclusion

In this paper we have proposed a low-complexity approximation of the MMSE-PIC detector for non-orthogonal waveforms, which bases on a sparse factorization of the equivalent channel matrix. With this approximation, the detection complexity becomes the same order as OFDM and the operation can be easily parallelized, allowing for low-latency high-throughput implementations. Simulations of achieved FER for MIMO-GFDM show only a negligible performance degradation compared to the exact MMSE-PIC detector, making the proposal a viable option for the implementation of future wireless communication systems.

In addition, we have thoroughly analyzed the FER performance of iterative MMSE-PIC and non-iterative LMMSE detectors for MIMO-GFDM under realistic channel conditions. We have investigated the performance when either using LDPC codes or convolutional codes (CCs) as the forward error correcting code. When using the CC, the combination of MIMO constellation constraint and CC can be considered as a serially concatenated code, which can eventually reach optimal performance with respect to the ML criterion. In this sense, we have shown that the application of CCs is superior to LDPC codes in terms of FER in iterative receiver structures. In particular, our simulations have shown that the CC in combination with the iterative MMSE-PIC receiver structure can reach the optimal ML decoding performance.

When comparing the FER performance of GFDM and OFDM, we have seen that for small subcarrier allocations, GFDM outperforms OFDM in the non-iterative receiver case. However, when more subcarriers are allocated, the non-iterative receiver cannot cancel all interference and GFDM becomes inferior. In contrast, when considering iterative MMSE-PIC structures, the additional ICI can be considered by the SISO demapper, eventually leading to a steeper slope of obtained FER curves compared to OFDM. With the iterative MMSE-PIC receiver, GFDM performed equal or even outperformed OFDM in various channel conditions. The findings make the proposed low-complexity MMSE-PIC demapper a viable method for the implementation of alternative waveforms for future wireless systems.

VII. Acknowledgements

The work presented in this paper was sponsored by the Federal Ministry of Education and Research within the programme "Twenty20 - Partnership for Innovation" under contract 03ZZ0505B - "fast wireless". The computations were performed at the Center for Information Services and High Performance Computing (ZIH) at TU Dresden.

Appendix

A. Proof of (25)

Starting from the biased LMMSE estimate of $\vec{D}$ from the received signal $\vec{y}$

$$\eta_D^p = \mu_D^a + \Sigma_D^a \mathbf{H}^{\mathrm{H}}(\mathbf{H}\Sigma_D^a\mathbf{H}^{\mathrm{H}} + \sigma^2\mathbf{I})^{-1}(\vec{y} - \mathbf{H}\vec{\mu}_D^a) \quad (42)$$

$$\Lambda_D^p = \Sigma_D^a - \Sigma_D^a\mathbf{H}^{\mathrm{H}}(\mathbf{H}\Sigma_D^a\mathbf{H}^{\mathrm{H}} + \sigma^2\mathbf{I})^{-1}\mathbf{H}\Sigma_D^a, \quad (43)$$

by assuming $\tilde{\mathbf{H}} = \mathbf{H}\mathbf{U}^{\mathrm{H}}$,$\vec{\mu}_d^a = \mathbf{U}^{\mathrm{H}}\vec{\mu}_D^a$ and $\Sigma_d^a = \mathbf{U}^{\mathrm{H}}\Sigma_D^a\mathbf{U}$ we calculate

$$\mathbf{U}^{\mathrm{H}}\eta_D^p = \vec{\mu}_d^a + \Sigma_d^a\tilde{\mathbf{H}}^{\mathrm{H}}(\tilde{\mathbf{H}}\Sigma_d^a\tilde{\mathbf{H}}^{\mathrm{H}} + \sigma^2\mathbf{I})^{-1}(y - \tilde{\mathbf{H}}\vec{\mu}_d^a) = \eta_d^p, \quad (44)$$

$$\mathbf{U}^{\mathrm{H}}\Lambda_D^p\mathbf{U} = \Sigma_d^a - \Sigma_d^a\tilde{\mathbf{H}}^{\mathrm{H}}(\tilde{\mathbf{H}}\Sigma_d^a\tilde{\mathbf{H}}^{\mathrm{H}} + \sigma^2\mathbf{I})^{-1}\tilde{\mathbf{H}} = \Lambda_d^p \quad (45)$$

Note that from (cf. (12))

$$(\Sigma_D^p + \Sigma_D^a)^{-1} = \mathrm{diag}(\mathbf{H}^{\mathrm{H}}(\mathbf{H}\Sigma_D^a\mathbf{H}^{\mathrm{H}} + \sigma^2\mathbf{I})^{-1}\mathbf{H}) \quad (46)$$

directly follows (cf. (11))

$$(\Sigma_D^p + \Sigma_D^a)^{-1}(\vec{\mu}_D^p - \vec{\mu}_D^a) = \mathbf{H}^{\mathrm{H}}(\mathbf{H}\Sigma_D^a\mathbf{H}^{\mathrm{H}} + \sigma^2\mathbf{I})^{-1}(\vec{y} - \mathbf{H}\vec{\mu}_D^a). \quad (47)$$

Now, by substituting (47) into (44) we end up with

$$\eta_d^p = \mathbf{U}^{\mathrm{H}}\eta_D^p = \vec{\mu}_d^a + \mathbf{U}^{\mathrm{H}}\Sigma_D^a(\Sigma_D^p + \Sigma_D^a)^{-1}(\vec{\mu}_D^p - \vec{\mu}_D^a) \quad (48)$$

$$= \vec{\mu}_d^a + \Sigma_d^a\mathbf{U}^{\mathrm{H}}(\mathbf{U}\Sigma_d^a\mathbf{U}^{\mathrm{H}} + \Sigma_D^p)^{-1}(\vec{\mu}_D^p - \mathbf{U}^{\mathrm{H}}\vec{\mu}_d^a). \quad (49)$$

Similarly, by using (46) in (45) we get

$$\Lambda_d^p = \mathbf{U}^{\mathrm{H}}\Lambda_D^p\mathbf{U} = \Sigma_d^a - \mathbf{U}^{\mathrm{H}}\Sigma_D^a(\Sigma_D^p + \Sigma_D^a)^{-1}\Sigma_D^a\mathbf{U} \quad (50)$$

$$= \Sigma_d^a - \Sigma_d^a\mathbf{U}^{\mathrm{H}}(\mathbf{U}\Sigma_d^a\mathbf{U}^{\mathrm{H}} + \Sigma_D^p)^{-1}\mathbf{U}^{\mathrm{H}}\Sigma_d^a \quad (51)$$

Now, comparing (49) and (51) with (25), the proof is finished.

References

[1] M. Simsek, A. Aijaz, M. Dohler, J. Sachs, and G. Fettweis, "5G-Enabled Tactile Internet," *IEEE Journal on Selected Areas in Communications*, vol. 8716, no. c, pp. 1–1, 2016.

[2] J. J. G. Andrews, S. Buzzi, W. Choi, S. V. S. Hanly, A. Lozano, A. A. C. K. Soong, and J. J. C. Zhang, "What will 5G be?" *IEEE Journal on Selected Areas in Communications*, vol. 32, no. 6, pp. 1065–1082, 2014.

[3] G. Wunder et. al., "5GNOW: non-orthogonal, asynchronous waveforms for future mobile applications," *IEEE Communications Magazine*, vol. 52, no. 2, pp. 97–105, feb 2014.

[4] P. Banelli, S. Buzzi, G. Colavolpe, A. Modenini, F. Rusek, and A. Ugolini, "Modulation formats and waveforms for 5G networks: Who will be the heir of OFDM?" *IEEE Signal Processing Magazine*, vol. 31, no. 6, pp. 80–93, 2014.

[5] N. Michailow et. al., "Generalized Frequency Division Multiplexing for 5th Generation Cellular Networks," *IEEE Transactions on Communications*, vol. 62, no. 9, pp. 3045–3061, 2014.

[6] A. M. Tonello and M. Girotto, "Cyclic block filtered multitone modulation," *EURASIP Journal on Advances in Signal Processing*, vol. 2014, no. 1, p. 109, 2014.

[7] D. Zhang, M. Matthé, L. L. Mendes, and G. Fettweis, "Message Passing Algorithms for Upper and Lower Bounding the Coded Modulation Capacity in a Large-scale Linear System," *IEEE Signal Processing Letters*, vol. 23, no. 4, pp. 537–540, 2016.

[8] F. Schaich, T. Wild, and Y. Chen, "Waveform Contenders for 5G - Suitability for Short Packet and Low Latency Transmissions," in *2014 IEEE 79th Vehicular Technology Conference (VTC Spring)*. IEEE, may 2014, pp. 1–5.

[9] A. Sahin and H. Arslan, "Edge windowing for OFDM based systems," *IEEE Communications Letters*, vol. 15, no. 11, pp. 1208–1211, 2011.

[10] J. Abdoli, M. Jia, and J. Ma, "Filtered OFDM: A new waveform for future wireless systems," *IEEE Workshop on Signal Processing Advances in Wireless Communications, SPAWC*, vol. 2015-Augus, pp. 66–70, 2015.

[11] Z. Zhao, M. Schellmann, Q. Wang, X. Gong, R. Boehnke, and W. Xu, "Pulse shaped OFDM for asynchronous uplink access," in *Asilomar Conference on Signals, Systems and Computers*, 2015, pp. 3–7.

[12] N. E. Tunali, M. Wu, C. Dick, C. Studer, and S. Jose, "Linear Large-Scale MIMO Data Detection for 5G Multi-Carrier Waveform Candidates," in *Asilomar Conference on Signals, Systems, and Computers*, 2015, pp. 1–5.

[13] M. Matthé, D. Zhang, and G. P. Fettweis, "Sphere-Decoding Aided SIC for MIMO-GFDM: Coded Performance Analysis," in *Wireless Communication Systems (ISWCS), 2016 International Symposium on*, Poznan, 2016, pp. 165–169.

[14] M. Matthé, I. Gaspar, D. Zhang, and G. Fettweis, "Short Paper: Near-ML Detection for MIMO-GFDM," in *Proceedings IEEE 82nd Vehicular Technology Conference*, Boston, 2015.

[15] B. Farhang-Boroujeny and H. Moradi, "Derivation of GFDM based on OFDM principles," in *2015 IEEE International Conference on Communications (ICC)*. IEEE, jun 2015, pp. 2680–2685.

[16] D. Zhang, M. Matthé, L. L. Mendes, and G. Fettweis, "A Markov Chain Monte Carlo Algorithm for Near-Optimum Detection of MIMO-GFDM Signals," in *IEEE 26th International Symposium on Personal, Indoor and Mobile Radio Communications - (PIMRC '15)*, 2015, pp. 281–286.

[17] D. Zhang et. al, "Expectation Propagation for Near-Optimum Detection of MIMO-GFDM Signals," *IEEE TRANSACTIONS ON WIRELESS COMMUNICATIONS*, vol. 15, no. 2, pp. 1045–1062, 2016.

[18] C. Studer, S. Fateh, and D. Seethaler, "ASIC implementation of soft-input soft-output MIMO detection using MMSE parallel interference cancellation," *IEEE Journal of Solid-State Circuits*, vol. 46, no. 7, pp. 1754–1765, 2011.

[19] W.-c. Sun, W.-h. Wu, C.-h. Yang, and Y.-l. Ueng, "An Iterative Detection and Decoding Receiver for LDPC-Coded MIMO Systems," *IEEE TRANSACTIONS ON CIRCUITS AND SYSTEMS*, vol. 62, no. 10, pp. 2512–2522, 2015.

[20] L. Fang, L. Xu, and D. D. Huang, "Low Complexity Iterative MMSE-PIC Detection for Medium-Size Massive MIMO," *IEEE Wireless Communications Letters*, vol. 5, no. 1, pp. 108–111, 2016.

[21] C. Studer and H. Bolcskei, "Soft–Input Soft–Output Single Tree-Search Sphere Decoding," *IEEE Transactions on Information Theory*, vol. 56, no. 10, pp. 4827–4842, oct 2010.

[22] E. P. Adeva and G. P. Fettweis, "Efficient Architecture for Soft-Input Soft-Output Sphere Detection With Perfect Node Enumeration," *IEEE Transactions on Very Large Scale Integration (VLSI) Systems*, pp. 1–14, 2016.

[23] G. M. Guvensen and A. O. Yilmaz, "A general framework for optimum iterative blockwise equalization of single carrier MIMO systems and asymptotic performance analysis," *IEEE Transactions on Communications*, vol. 61, no. 2, pp. 609–619, 2013.

[24] D. Zhang, M. Matthe, L. L. Mendes, and G. P. Fettweis, "A Study on the Link Level Performance of Advanced Multicarrier Waveforms under MIMO Wireless Communication Channels," *IEEE Transactions on Wireless Communications*, vol. PP, no. 99, 2017.

[25] M. Matthé, D. Zhang, and G. Fettweis, "Iterative Detection using MMSE-PIC Demapping for MIMO-GFDM Systems," in *IEEE European Wireless (EW '16)*, 2016.

[26] S. Benedetto, G. Montorsi, D. Divsalar, and F. Pollara, "Iterative Decoding of Serially Concatenated Codes with Interleavers and Comparison with Turbo Codes," *Proc. ¯IEEE Global Telecommunications Conference*, pp. 654–658, 1997.

[27] N. Michailow, S. Krone, M. Lentmaier, and G. Fettweis, "Bit Error Rate Performance of Generalized Frequency Division Multiplexing," in *2012 IEEE Vehicular Technology Conference (VTC Fall)*. IEEE, sep 2012, pp. 1–5.

[28] S. M. Kay, *Fundamentals of Statistical Signal Processing: Estimation Theory*, ser. Prentice Hall Signal Processing Series. Prentice Hall, 1993, no. v. 1.

[29] M. Huemer and O. Lang, "On component-wise conditionally unbiased linear Bayesian estimation," *Conference Record - Asilomar Conference on Signals, Systems and Computers*, vol. 2015-April, pp. 879–885, 2015.

[30] M. Huemer, O. Lang, and C. Hofbauer, "Component-wise conditionally unbiased widely linear MMSE estimation," *Signal Processing*, vol. 133, no. October 2016, pp. 227–239, 2017.

[31] C. Studer, "Iterative MIMO Decoding: Algorithms and VLSI Implementation Aspects," vol. 202, 2009.

[32] S. S. Das and S. Tiwari, "Discrete Fourier transform spreading-based generalised frequency division multiplexing," *IEEE Electronics Letters*, vol. 51, no. 10, 2015.

[33] M. K. Ho and M. K. Ng, "Splitting iterations for circulant-plus-diagonal systems," *Numerical Linear Algebra with Applications*, vol. 12, no. 8, pp. 779–792, 2005.

[34] G. H. Golub and C. F. V. Loan, *Matrix Computations*, 1996.

[35] M. Matthé, N. Michailow, I. Gaspar, and G. Fettweis, "Influence of Pulse Shaping on Bit Error Rate Performance and Out of Band Radiation of Generalized Frequency Division Multiplexing," in *ICC'14 - Workshop on 5G Technologies (ICC'14 WS - 5G)*, Sydney, Australia, 2014, pp. 43—-48.

[36] S. ten Brink, "Convergence of iterative decoding," *IEEE Electronics Letters*, vol. 35, no. 10, pp. 806–808, 1999.

[37] S. T. Brink, "Convergence behavior of iteratively decoded parallel concatenated codes," *IEEE Transactions on Communications*, vol. 49, no. 10, pp. 1727–1737, 2001.

[38] A. Ibing and H. Boche, "On predicting convergence of iterative MIMO detection-decoding with concatenated codes," *IEEE Transactions on Vehicular Technology*, vol. 59, no. 8, pp. 4134–4139, 2010.

[39] A. Elkhazin, K. Plataniotis, and S. Pasupathy, "Irregular convolutional codes in multiantenna bit-interleaved coded modulation under iterative detection and decoding," *IEEE Transactions on Vehicular Technology*, vol. 59, no. 7, pp. 3332–3341, 2010.

[40] S. Benedetto, D. Divsalar, G. Montorsi, and F. Pollara, "Serial concatenation of interleaved codes: Performance analysis,design, and iterative decoding," *IEEE Transactions on Information Theory*, vol. 44, no. 3, pp. 909–926, 1998.